

Tuning Intermolecular Interaction Between Lignin and Carbon Nanotubes in Fiber Composites – A Combined Experimental and *Ab-Initio* Modeling Study

Jan Badorrek^{1,2}, Michael Walter^{3,4,*} and Marie-Pierre Laborie^{1,2,*}

¹Freiburger Materialforschungszentrum, Stefan-Meier-Straße 21, D-79104 Freiburg im Breisgau, Germany

²Chair of Forest Biomaterials, Werthmannstraße 6, D-79085 Freiburg im Breisgau, Germany

³Freiburg Center for Interactive Materials and Bioinspired Technologies (FIT), Georges-Köhler-Allee 105, D-79110 Freiburg im Breisgau, Germany

⁴Fraunhofer Institute for Mechanics of Materials (IWM), Wöhlerstraße 11, D-79108 Freiburg im Breisgau, Germany

Received June 28, 2017; Accepted November 11, 2017

ABSTRACT: Doping lignin with carbon nanotubes is a promising strategy for cost-effective high-performance carbon fibers. We investigate the intermolecular interaction potential of CNT and organosolv lignin with two main approaches. Experimentally, oxidized purified multiwalled carbon nanotubes (MWCNTs) and beech organosolv lignins and derivatives are analyzed with their Hansen solubility parameters (HSPs) to assess their mutual compatibility. Theoretically, dispersion-corrected density functional theory simulations of the interaction between model molecules and single-walled carbon nanotubes reveal the source of interactions. We find that oxidation enables and enhances the interaction between carbon nanotubes and organosolv lignin experimentally, which is in agreement with the enhanced polar interaction found in the simulations.

KEYWORDS: CNT, DFT, Hansen solubility parameters, lignin, oxidation

1 INTRODUCTION

Carbon fiber (CF) polymer composites are valuable high-performance materials [1]. Their application is currently restricted to niche industries; their manufacturing price—which is strongly coupled with the CF-precursor cost—remains high [2]. If the current petroleum-based precursor polyacrylonitrile (PAN) would, however, be replaced with a cheaper, renewable alternative, carbon fibers could potentially be introduced into high-volume markets.

Lignin—a renewable, highly condensed and highly branched phenylpropanoid polymer—is incorporated into all plants as a compression strength agent [3–5]. This enormous abundance has caused large-scale research and effort to utilize lignin in mass-market products, e.g., in polymers or as a specialty chemical feedstock [6, 7]. Lignin exhibits many functional groups; besides a vast array of interunit bonds [8], aliphatic and aromatic OH groups are the most prominent ones. The production of CF from lignin in

particular has been researched and developed since the 1960s [1]. In a recent patent, Baker *et al.* claim strong benefits when carbon nanotubes (CNTs) were included in melt-spun lignin-based carbon fiber precursors; the final carbon fiber exhibited a 20% increase in strength as well as a 50% higher modulus [9].

CNTs are small carbonaceous tubes with a diameter in the nanometer range; they possess a very high aspect ratio [10]. Depending on their synthesis, they appear as single- or multiwalled carbon nanotubes (SWCNT and MWCNT resp.). Radushkevich and Lukynovich were the first to depict MWCNT [11, 12]. After Iijima's publication in 1991, a tremendous surge of research on CNTs and their utilization occurred [10, 13]. CNTs are generally known for their ability to enhance the mechanical properties of polymer composites they are embedded in [14].

In a follow-up to the patent mentioned above, the authors proposed that poor interfacial adhesion, however, limited the mechanical reinforcement of CNT [2]. Other researchers also encountered challenges when incorporating CNT into lignin-based CF precursor blends; these studies all suggest that the understanding and tuning of CNT-lignin interactions is critical to the optimum utilization of CNTs in lignin-based

*Corresponding authors: michael.walter@mf.uni-freiburg.de; marie-pierre.laborie@biomat.uni-freiburg.de

DOI: 10.7569/JRM.2017.634183

carbon fibers [15, 16]. In principle, the aromatic properties of lignin and its many OH groups are expected to be the main interaction partners of the CNT.

The interaction potential of CNT is either investigated experimentally or *in silico*. In computational studies, researchers investigate CNTs and their interaction by means of adsorption simulations. The simplest of such simulations deals with the adsorption of simple gases, e.g., O₂ and N₂ [17–20]. When researchers explicitly want to scrutinize the π - π interactions of CNT, benzene is chosen as the interaction probe [21, 22]. More complex adsorption simulations have been performed by Kumar *et al.*, who investigated the interaction of carbohydrate models with simplified CNT and graphene models [23]. Finally, bulk properties related to interaction potential were calculated by Lee and coworkers, who used molecular dynamics to compute solubility parameters for a variety of model CNTs [24].

Experimentally, nanotubes and their surfaces are often modified and functionalized by mechanical, physicochemical or irradiation methods to improve their interaction potential [25]. More specifically, oxidation treatments are a popular choice to introduce surface functions—they alter the noncovalent interactions of the CNT and also present a basis for further modifications [25, 26]. OH groups, aldehydes and carboxylic acids are typical representatives of the many oxygen-bearing surface functionalities commonly found on CNT [27]. To introduce these surface functionalities, various oxidizing agents, such as nitric acid [27] or ambient air, are employed [28–30]. The effect of nitric acid treatments on the interaction potential of nanotubes was quantified by Detriche *et al.* as well as Brandão *et al.* — they used the Hansen solubility parameter concept [31, 32].

The modes of CNT-lignin interaction—the initial topic of interest—have been proposed for MWCNT-Kraft lignin systems through dispersion experiments coupled with Raman spectroscopy. The researchers determined π - π bonding to be the main contribution to the noncovalent interaction systems [33, 34]. Hydrogen bonding between the lignins' OH groups and the nonfunctionalized nanotubes' surface played a passive role [34].

To the best of our knowledge there are no accounts on how oxidation of CNT can be employed to improve the interaction potential between CNT and lignin. The overall goal of this article is to gain insight into the impact of CNT oxidation treatment on its potential adhesion and adsorption to lignin and lignin model compounds. We therefore determine bulk indicators of compatibility for organosolv lignin and several oxidized MWCNTs using Hansen solubility parameters. In a second step, we approximate the different modes of CNT-lignin interaction by adsorption of small model molecules

on pristine and defective CNT. In particular, we focus on possible interactions between OH-containing CNT and simple cyclic model compounds mimicking common lignin functional groups. Finally, we compare the experimental and theoretical approaches.

2 METHODOLOGY

2.1 Materials

Beech organosolv lignin with an Mw of 4300 g/mol and a PDI of 3.9 was supplied by Fraunhofer CBP (Leuna, Germany). Thermally purified multiwalled carbon nanotubes (MWCNT; Graphistrength C100 HP) were supplied by Arkema, France. They were weighed into 6 g batches (divided into 6 small porcelain dishes) and were oxidized in a muffle oven at 600 °C for varying times. After the heat treatment, they were quenched in an excess of deionized water and subsequently freeze-dried to yield oxidized multiwalled carbon nanotubes (o-MWCNTs).

2.2 HSP Determination

Predictions on the miscibility and compatibility of two substances can be derived from the Flory-Huggins theory [35, 36], where the free energy of mixing is derived from the number of moles n_i , the volume fraction ϕ_i and the interaction parameter χ_{12} :

$$\Delta G_m = RT [n_1 \ln \phi_1 + n_2 \ln \phi_2 + n_1 \phi_2 \chi_{12}] \quad (1)$$

where R is the universal gas constant and T is the temperature. The interaction parameter χ_{12} is given by:

$$\chi_{12} = \chi_H + \chi_S = \frac{V_m}{RT} (\delta_1 - \delta_2)^2 + \chi_S \quad (2)$$

where χ_H and χ_S are the contributions to the total interaction parameter due to enthalpy and entropy; V_m is the molar volume and $\delta_{i,i=1,2}$ are the Hildebrand solubility parameters. The latter are equal to the square root of the cohesive energy density [37]:

$$\delta_i = \sqrt{\frac{\Delta H_v - RT}{V_m}} = \sqrt{\frac{E_{coh}}{V_m}} \quad (3)$$

Here, ΔH_v represents the heat of vaporization and E_{coh} is the cohesive energy. The latter is determined as the sum of all noncovalent bonds.

Miscible pairs are characterized by a small χ_{12} , viz., a close similarity in solubility parameters. Therefore, comparing the solubility parameters of two compounds provides information on their theoretical miscibility, viz., their mutual compatibility.



Hildebrand's solubility parameter was deconvoluted by Hansen into three components, representative of three possible types of intermolecular interactions [38]:

$$\delta^2 = \delta_D^2 + \delta_p^2 + \delta_H^2 \quad (4)$$

where δ_D is the contribution due to dispersion forces, δ_p the contribution due to polar interaction and δ_H the contribution due to hydrogen bonding and other electronic effects [38, 39]. When molar volumes—and by extension χ_{12} —are not easily accessible, the Hansen solubility parameters also offer a solution to predict and quantify bulk interactions; this is the case in our work.

To judge the compatibility of the organosolv lignin with the (o-)MWCNT, we use Hansen's relative energy distance (*RED*) given by:

$$RED = \frac{R_a}{R_0} = \frac{\sqrt{4(\delta_{D2} - \delta_{D1})^2 + (\delta_{p2} - \delta_{p1})^2 + (\delta_{H2} - \delta_{H1})^2}}{R_0} \quad (5)$$

where R_a is the distance between the centers of the two solubility spheres and R_0 is the experimentally determined radius of the lignin's solubility sphere [38]. If $RED < 1$, then two substances are compatible—at least one center of a HSP sphere lies within the other HSP sphere. If $RED_{A+B} < RED_{A+C}$, then *A* and *B* are more compatible with each other than *A* and *C*.

The solubility parameters of the organosolv lignin and all MWCNT samples were determined according to Hansen's method [38]. We attempted to dissolve and disperse, respectively, all samples at a concentration of 1 mg/mL. After 24 h, the suitability of the solvents to dissolve or disperse the given samples was evaluated. The solvent table can be found in the Supplementary Data.

2.3 DFT Simulation

The DFT adsorption simulations were realized within the grid-based GPAW package [40, 41]. The structures were set up within a supercell of 48 Å in both *x* and *y* directions. Periodic boundary conditions were applied in the direction of the tube—the *z* direction, ~12.3 Å in length—and zero boundary conditions in perpendicular directions. The simulation grid contained 256 grid points in both *x* and *y* directions as well as 64 grid points in *z* direction. Due to the grid-based nature of GPAW, basis-set superposition errors were of no concern.

All structures were optimized until a force gradient of 0.02 eV/Å was reached. The total energies were calculated with a TS09-corrected PBE exchange-correlation functional [42, 43].

An (8,8) armchair single-wall carbon nanotube (SWCNT) with a diameter of 10.8 nm was used as a model for the carbon nanotubes. The unit cell contained 5 repetition units of ~12.3 nm length pointing in *z* direction. The surface structure was also altered. Either the nanotube exhibited a pristine surface (SWCNT) or a Stone-Wales defect aligned oblique to the SWCNT axis (sw-SWCNT). The latter represents an important class of in-plane defects commonly found in CNT [44]. As a third surface variation, the nanotube was functionalized with a hydroxyl group (o-SWCNT) in order to mimic one of the various effects of CNT oxidation [28]. There are many other oxygen-bearing functional groups encountered in CNT [27] that could be subject to further investigations. The same is true for structural defects arising through oxidation [28].

The adsorption energies E_{ads} of six small cyclic probe molecules (cyclohexane, cyclohexanol, methoxycyclohexane, benzene, phenol, anisol) on the SWCNT were calculated. E_{ads} is defined as the difference between the total energies of the adsorption complex $E_{A+B,TS09}$ and the sum of the individual reactants' total energies $E_{A,TS09}$ and $E_{B,TS09}$; as indicated, these energies were calculated at the TS09-level:

$$E_{ads} = E_{A+B,TS09} - (E_{A,TS09} + E_{B,TS09}) \quad (6)$$

Similarly, we calculated the E_{ads} of a p-SWCNT dimer, of an sw-SWCNT adsorbing on an SWCNT and of an o-SWCNT adsorbing onto an SWCNT.

The adsorption energy E_{ads} is composed of approximately four contributions stemming from different fundamental noncovalent interactions [23, 45, 46]:

$$E_{ads} = E_{electrostatic} + E_{induction} + E_{exchange-repulsion} + E_{dispersive} \quad (7)$$

The first three terms on the right-hand side are included in the total adsorption energies calculated at the PBE level. We summarize them within the term E_{polar} :

$$E_{polar} = E_{electrostatic} + E_{induction} + E_{exchange-repulsion} = E_{A+B,PBE} - (E_{A,PBE} + E_{B,PBE}) \quad (8)$$

Finally, $E_{dispersive}$ can be derived from the difference of E_{ads} and E_{polar} :

$$E_{dispersive} = E_{ads} - E_{polar} \quad (9)$$

Prior to the actual adsorption simulations, the convergence of E_{ads} with respect to *k*-points in *z* direction was investigated in a smaller supercell (24 Å × 24 Å × ~13.3 Å) with identically spaced grid points (128 × 128 × 64). It became clear that the Γ -point is already

sufficient to achieve convergence of E_{ads} of benzene on a (4,4)-SWCNT within 1 meV. Similarly, the influence of the periodic boundary conditions on the isolated benzene molecule was found to be less than 1 meV.

3 RESULTS

3.1 HSP Determination

The experimental dissolution/dispersion data was fit with the single-sphere genetic algorithm supplied by HSPiP 5.0.06. The resulting HSPs of (o-)MWCNT are depicted against the oxidation treatment time in Figure 1a. We find that the initial MWCNTs are characterized by slightly larger dispersive, but fundamentally lower polar and hydrogen bonding parameters than those found in the organosolv lignin (see Table 1). Their pairwise RED is equal to 1.3, suggesting low dispersibility of MWCNT in lignin.

With increasing oxidation time, the nanotubes' δ_D decreases while δ_p and δ_H increase (see Figure 1a). This

is expected: an increase in oxygen-bearing surface functional groups is supposed to enhance the nanotubes' surface polarity and hydrogen bonding capacity. The decrease in δ_D suggests that the nanotubes' π -clouds are successively being rendered sterically inaccessible. Most probably, the growing amount of OH groups presents a steric hindrance.

Thus, the o-MWCNTs at first become more similar in properties to the organosolv lignin, facilitating compatibility after 30 min of treatment time. Intermediate oxidation times of around 45 min yielded the best compatibility (RED = 0.32) in this work.

From Figure 1a it is not clear whether a convergence in HSP is reached for the o-MWCNT after 45 min. With a treatment time of 45 min or higher, o-MWCNTs group to the right of the organosolv lignin's HSP sphere center, as shown in Figure 1b. o-MWCNTs with a treatment time of 30 min or lower group to the left.

Detriche *et al.* proposed a two-sphere HSP fit to gain insight into the dispersion behavior of oxidized CNT [32]. When treating our datasets of o-MWCNT with the two-sphere genetic model supplied by the HSPiP

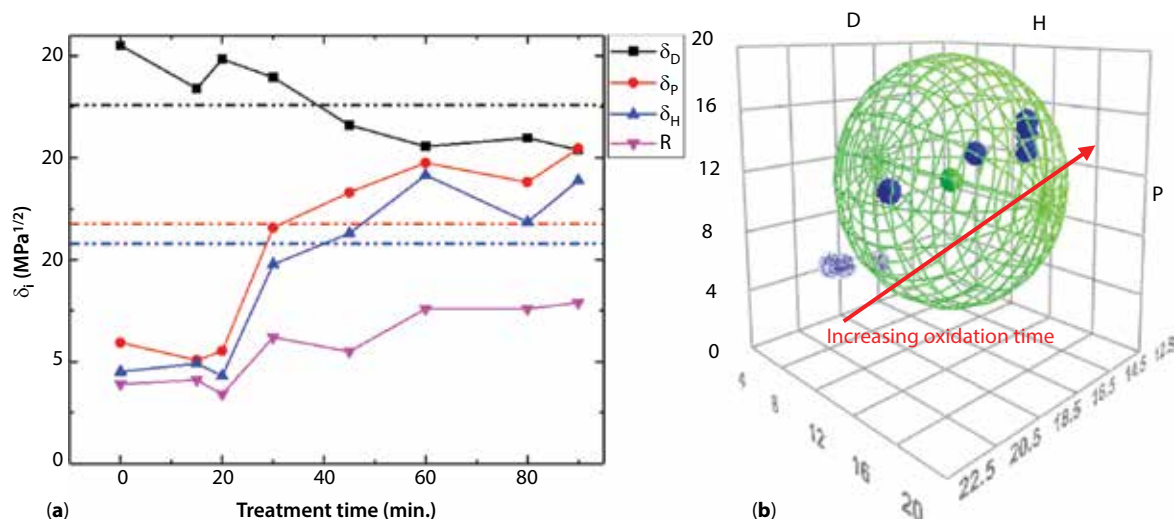


Figure 1 (a) Influence of treatment time on the Hansen solubility parameters of o-MWCNT. The broken line represents the respective HSP (on top, δ_D is in black, in the middle, δ_p is shown in red and on the bottom δ_H is plotted in blue) of the organosolv lignin. (b) HSP sphere of organosolv lignin (large sphere) and (o-)MWCNT (small spheres). Wired MWCNT spheres lie outside of the green organosolv lignin's solubility sphere while solid MWCNT spheres lie inside, indicating good interactions in the latter case. The red arrow indicates increasing oxidation time of the o-MWCNT.

Table 1 Hansen solubility parameters of organosolv lignin as well as selected (o-)MWCNT.

Sample	δ_D [$\text{MPa}^{1/2}$]	δ_p [$\text{MPa}^{1/2}$]	δ_H [$\text{MPa}^{1/2}$]	R [$\text{MPa}^{1/2}$]
Organosolv lignin	17.6	11.8	10.8	8.0
MWCNT	20.5	5.9	4.5	3.9
o-MWCNT (90 min)	15.4	15.4	13.8	7.9

software, our results are much alike (see Figure 2): one sphere is characterized by a high δ_D ($\sim 20 \text{ MPa}^{1/2}$), but low δ_p , δ_H and R (each around $5 \text{ MPa}^{1/2}$). This first sphere represents the still unmodified MWCNT fraction. The second sphere displays a slightly lower δ_D ($\sim 17 \text{ MPa}^{1/2}$), while δ_p and δ_H are now much higher ($\sim 15 \text{ MPa}^{1/2}$ and $\sim 12 \text{ MPa}^{1/2}$ resp.)—this represents the functionalized nanotube fraction. Conclusively, the overall—single-sphere—HSP of (o-)MWCNT is dominated by the unmodified fractions at lower oxidation times. The influence of the modified fractions is overwhelming at higher treatment times.

Thermal oxidation of MWCNT with air—followed by quenching in water—therefore facilitates good interaction between CNT and organosolv lignin. We could not determine whether prolonged treatment times enhance the interaction further. In order to understand the underlying molecular scale phenomena, we report selected results from a computational adsorption study of simplified lignin model molecules on SWCNT in the next section. The full study will be published elsewhere.

3.2 Adsorption Simulation

3.2.1 Pristine SWCNT (and Stone-Wales SWCNT)

We have modeled the adsorption behavior of six cyclic model molecules on pristine (8,8)-SWCNT as a model to mimic the interactions between pristine MWCNT and lignin in a strongly simplified manner. We use six probe molecules that were selected in order to cover the various small structural motives which can be found in lignin. Phenol and anisol are representatives of lignin's ubiquitous substituted phenyl rings. Cyclohexanol serves as a model for the aliphatic OH-functions. Cyclohexane exemplifies the sp^3 -hybridized carbons of the side-chains. Benzene is a model for the sp^2 -hybridized carbon atoms in either the side-chains or in the phenyl rings and methoxycyclohexane serves as the aliphatic counterpart of anisol.

The total adsorption energies E_{ads} of these molecules interacting with the pristine SWCNT are shown in Figure 3. All six probe molecules are attracted by the SWCNT as evidenced by the negative total adsorption

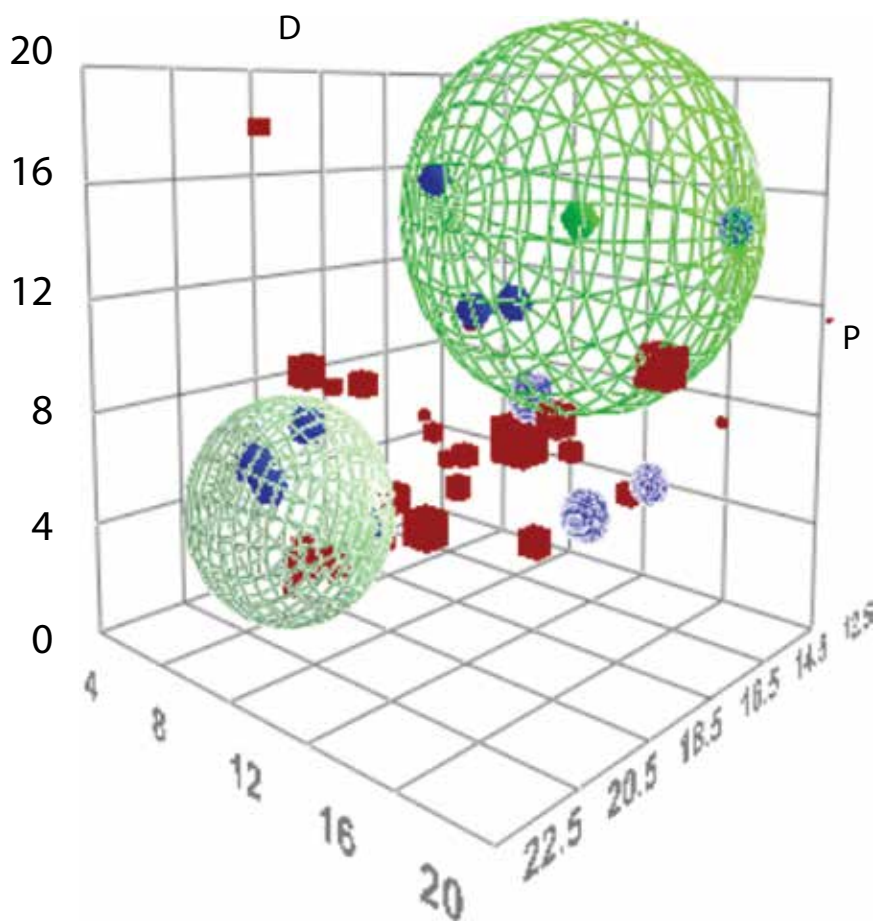


Figure 2 A two-sphere HSP fit to raw solubility data (sphere = good solvent, box = red solvent) according to Detriche *et al.* [32]. The dataset shown was recorded for o-MWCNT treated for 90 min.

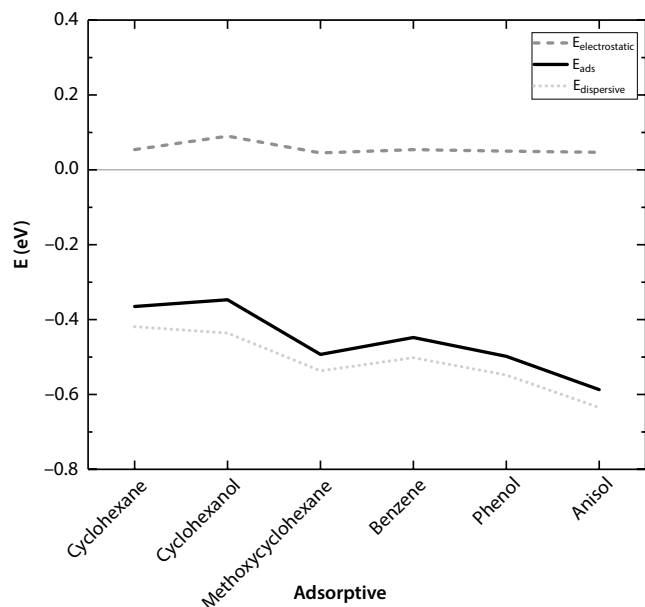


Figure 3 Adsorption energies of small molecules on a (8,8) p-SWCNT. The adsorption energies due to electrostatic interactions E_{polar} are depicted in dark gray, the total adsorption energies E_{ads} are given in solid black lines and the adsorption energies due to dispersive interactions $E_{\text{dispersive}}$ are plotted in light gray.

energies E_{ads} . All adsorption complexes were found to be most stable when the probe molecules were aligned parallel to the surface of the SWCNT, in agreement with what has already been reported for benzene [47].

The lowest binding is found in cyclohexane and the changes in binding energy relative to this molecule can be understood as follows. Attractive interaction is virtually unchanged upon addition of an OH group (cyclohexanol, only ~ 20 meV difference). Roughly ~ 100 meV is gained by either adding a methoxy group (methoxycyclohexane) or by reducing the six-ring to benzene, which introduces aromaticity. Combining both aromaticity and functional groups on the six-ring, the adsorption is enhanced by up to ~ 200 meV as compared to cyclohexane. With exception of the sp^3 -hybridized carbons, all structural motifs in lignin— i.e., the sp^2 -hybridized carbons, hydroxyl and methoxyl groups as well as combinations thereof—are thus good interaction partners for the pristine surface sections of CNT.

Energy deconvolution in Figure 3 reveals the dominating effect of the dispersive interaction on the total adsorption energy between probe molecules and the p-SWCNT. In contrast, the polar contribution is found to be always positive, i.e., nonbinding. Similar observations were reported by Kumar *et al.* [23] as well as by Hassan *et al.* [48]. The observed binding energy trends were not altered significantly with the introduction of

the Stone-Wales defect into the SWCNT (not shown; details will be published elsewhere). Therefore, such in-plane defects have little effect on the CNT-lignin interaction potential.

3.2.2 SWCNT Functionalized with OH Groups

Having gained a basic understanding of the adsorption energy between pristine SWCNT and our model compounds, we turn to adsorption on o-SWCNTs. All molecules were set up to adsorb directly onto the top of the OH group, therefore mimicking a nanotube's surface densely functionalized with a less accessible carbon backbone. The respective binding energies are shown in Figure 4.

The introduction of the OH group changes the interaction behavior substantially. Generally, E_{ads} is strongly reduced, except for cyclohexanol and methoxycyclohexane. These two molecules gain binding energy by forming hydrogen bonds while resting on top of the OH group (see Figure 5a). Similarly, phenol does not align anymore to the nanotubes surface, but remains erect above the OH-function, having also formed a hydrogen bond (Figure 5c). The total adsorption energy of all aromatic compounds bound to o-SWCNTs is clearly lower than when bound to pristine SWCNT.

Apart from the actual structures, these changes can also be observed in the deconvoluted energies: the hydrogen-bonding complexes—formed between the o-SWCNT and cyclohexanol, methoxycyclohexane or phenol—exhibit attractive polar interaction as reflected by negative, i.e., binding E_{polar} , compared to the respective SWCNT complexes. However, these energetic gains do not compensate for the substantial loss in dispersive attractive interaction as $E_{\text{dispersive}}$ declines by up to ~ 500 meV. The reduction in $E_{\text{dispersive}}$ interaction towards o-SWCNT is particularly pronounced for the aromatic compounds, explaining the overall loss of attractive total E_{ads} . A similar effect was reported by Kumar *et al.*, who observed that the total binding energy of carbohydrate-CNT-model complexes diminishes by 100 to 200 meV when OH- π -binding is enforced, as the dispersive binding component diminished by up to 400 meV [23].

This is not surprising: the London-type interactions, from which $E_{\text{dispersive}}$ stems, diminish proportional to the sixth power of the inverse distance between the interacting partners and are thus short-ranged [43, 49]. The OH group acts as a spacer between the probe molecules and the nanotube surface, interfering with dispersive adsorption interaction due to steric hindrance [48].

These results indicate that if lignin is made to adsorb directly onto a CNT with a densely functionalized surface, the overall attractive interaction is diminished in

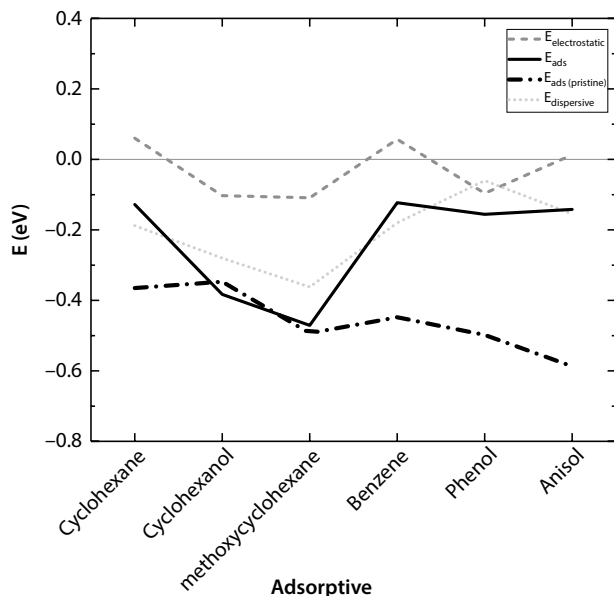


Figure 4 Adsorption energies of small molecules on an (8,8) o-SWCNT. The adsorption energies due to electrostatic interactions E_{polar} are depicted in dark gray, the total adsorption energies E_{ads} are given in solid black lines and the adsorption energies due to dispersive interactions $E_{\text{dispersive}}$ are plotted in light gray. The half-broken black line represents E_{ads} on SWCNT; the data is taken from Figure 3.

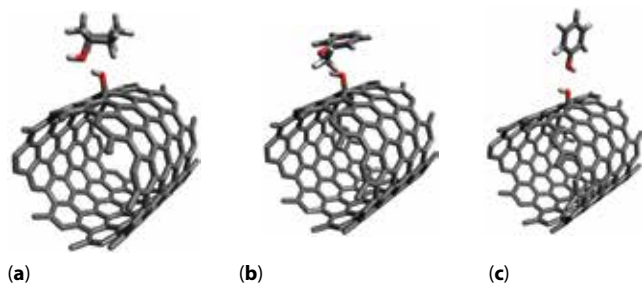


Figure 5 Adsorption complexes of (8,8) o-SWCNT and (a) cyclohexanol, (b) anisol or (c) phenol.

comparison to adsorption on the pristine CNT because the additional hydrogen bonding does not compensate dispersion interaction losses. For lesser degrees of surface functionalization, where lignin could adsorb dispersively between the OH-functions, the additional hydrogen bonding—exemplified by the phenol-o-SWCNT adsorption complex—can slightly strengthen the adsorption.

In summary, a favorable adsorption energy in pristine SWCNTs stems mostly from dispersive energy. $E_{\text{dispersive}}$ is enhanced by sequential functionalization of a cyclic alkane with functional groups commonly found in lignin. These include hydroxyl and methoxy groups as well as sp^2 -hybridized carbons. For o-SWCNTs, the total adsorption energy to model compounds is overall less favorable than for p-SWCNTs. In particular,

aromatic compounds lose attractive dispersive forces due to steric hindrance. H-bonding adds to E_{polar} , but is not strong enough to compensate the attraction losses fully.

3.2.3 Effect of Defects and Functionalization on CNT Aggregation

Two SWCNT aggregates are shown in Figure 6. They exhibit slight ring deformation, even after the structures were relaxed. Nevertheless, these aggregates serve as simple models to understand the effect of surface functional groups in SWCNT and, by extension, MWCNT self-aggregation.

The deconvoluted total adsorption energies E_{ads} of SWCNT aggregates are given in Table 2. Similar as in binding to molecules, Stone-Wales defects have only marginal influence on the binding energies. In contrast, aggregation is severely impeded by out-of-plane defects that hinder the SWCNT approach to dispersion interaction distance. Therefore, CNT-oxidation simultaneously interferes heavily with CNT self-aggregation, which in turn boosts the relative favorability of CNT-lignin complexes over CNT-CNT aggregates.

With this *in-silico* understanding of the effect of OH-functionalization of SWCNTs on adsorption energy with lignin models, we now turn to seeing how these theoretical predictions are connected to the experimental determinations of compatibilities.

3.3 Connection of Experiment and Theory

To better compare the results of our simulations with our experiments, we reduce the initially three-dimensional Hansen parameter into two dimensions by summing up polarization and hydrogen bonding contributions to [50]:

$$\delta_a^2 = \delta_p^2 + \delta_H^2 \quad (10)$$

These parameters are compiled in Table 3 for MWCNT variants and our model compounds. Please note that methoxycyclohexane's values were calculated with the Y-MB algorithm supplied with the HSPiP software (v5.0.06) since no experimental data was available. The table shows that the large δ_D of MWCNTs is reduced in o-MWCNT and that this effect is opposite for δ_a .

Gauging the interaction between two partners in the now two-dimensional solubility parameter space is done by determining the absolute energy distance between the two partners:¹

¹We can only determine the *absolute*, and not the *relative* energy distance, because we are missing the solubility radii R_0 .

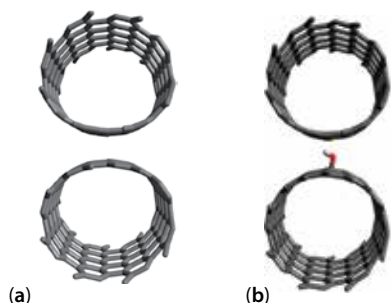


Figure 6 (a) Model dimer of pristine (8,8)-SWCNT viewed along the length of the nanotubes. (b) Model dimer of pristine and o-SWCNT.

Table 2 Energetics of different SWCNT aggregates. Pristine (SWCNT), SWCNT with Stone-Wales defects (sw-SWCNT) and OH-surface functions (o-SWCNT) are considered.

CNT aggregate	E_{ads} [eV]	E_{polar} [eV]	$E_{dispersive}$ [eV]
SWCNT vs. SWCNT	-1.44	1.16	-2.59
sw-SWCNT vs. SWCNT	-1.37	1.12	-2.49
o-SWCNT vs. SWCNT	-0.29	1.00	-1.29

$$AED = \sqrt{4(\delta_{D,1} - \delta_{D,2})^2 + (\delta_{a,1} - \delta_{a,2})^2} \quad (11)$$

In accordance with Hansen, we did not just define AED as the geometric distance between the two inter-actants, but opted to also double the weight of the $\delta_{D,i}$ difference [38].

We also list our binding energies between CNTs and the model molecules from the previous sections. In Table 3, the largest variations are found within binding to o-MWCNT. With the exception of methoxycyclohexane, the o-MWCNT binding energies anticorrelate to the δ_a values. We analyze this effect further below.

The AED and E_{ads} dataset of o-MWCNT—with 90 min treatment time—and o-SWCNT, respectively, do not correlate², as is depicted in Figure 7. No equivalent linear correlation occurs for the case of pristine and non-oxidized CNT, respectively. Similar to Lee *et al.*, we surmise that simulations employing perfect SWCNT do not fully model real non-functionalized nanotubes; real-world imperfections like residual catalysts or random functionalization are neglected [24]. Since our DFT simulations involving sw-SWCNT

²Note that the datapoint for methoxycyclohexane was not considered in the fit since the HSP values used were only predicted. Especially for δ_p , δ_H , and thus for δ_a , predictions can lack reliability [50].

yielded results very similar to those with pristine SWCNT, in-plane defects in the outer walls of the CNT are not the cause for these deviations.

The non-correlation between AED and binding energies is not surprising as these are different quantities and cannot be directly compared. Binding energies are more related to the squared Hildebrand solubility parameters, which are energy densities (cf. Equation 3). In the special case of o-MWCNT the AED is mainly determined by the difference in δ_a as the probe molecules show large variations in this quantity. They differ much less in δ_D , which is furthermore rather similar to o-MWCNT. As δ_a in o-MWCNT exceeds all molecular δ_a (cf. Table 3), the molecular δ_a practically determines the AED .

The δ_a itself is determined by the polarization contribution E_{polar} . In order to compare these quantities directly we need to scale the binding energy by a volume. For simplicity, we use the solvent excluded volume [51] of benzene in water, $V_{benzene} = 133 \text{ \AA}^3$, for all probe molecules. Figure 7b shows that the molecu-

lar δ_a^2 and $\frac{E_{polar}}{V_{benzene}}$ are indeed closely related even on

a quantitative level. In practical terms, this translates to the strength of the noncovalent OH-X bond being determined by the nature of the adsorbing molecule with the o-SWCNT's contribution remaining constant.

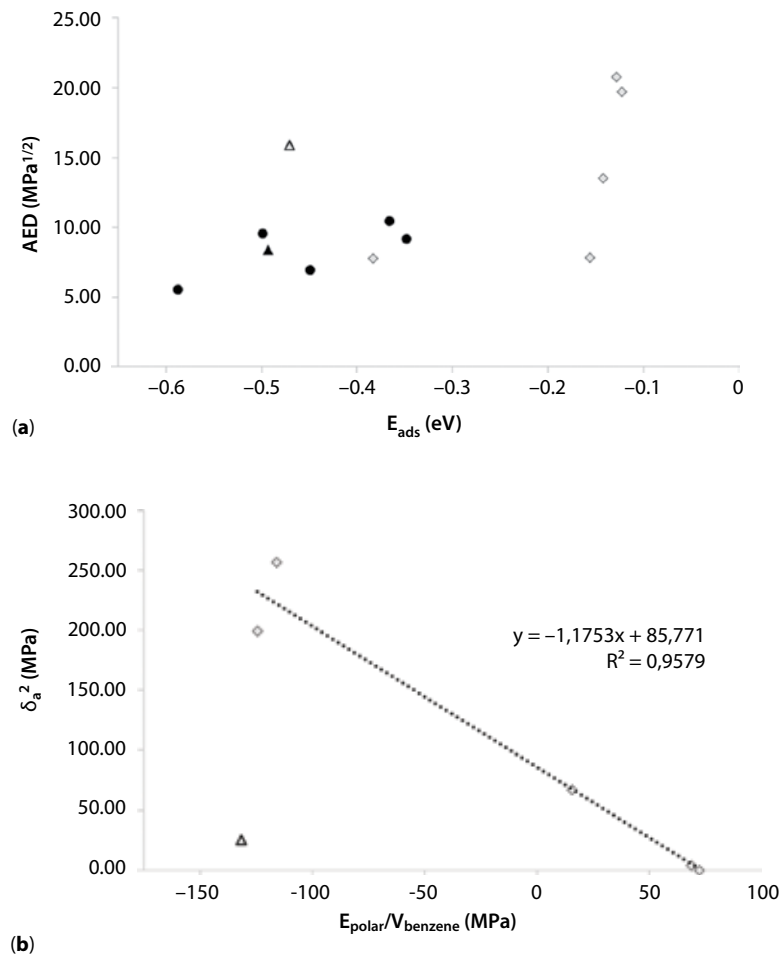
4 CONCLUSIONS

In this article, we reported on our efforts in controlling and understanding the interface of organosolv lignin and pristine and oxidized carbon nanotubes. Experimentally, we found that pristine MWCNTs do not favorably mix with lignin, while intermediate degrees of MWCNT oxidation significantly enhance the MWCNT-lignin interaction potential.

These experiments were amended by DFT-adsorption simulations using model molecules—containing basic functional groups that appear in lignin—and pristine as well as functionalized SWCNT. We found that the interaction to pristine SWCNTs is enhanced by OH or methoxy groups and by aromaticity. Functional groups on o-SWCNTs reduce the interaction due to steric hindrance. While there is no direct connection between DFT binding energies and RED for pristine SWCNT or oxidized SWCNT, the δ_a^2 of the six probe molecules could be quantitatively related to the polar binding contribution from our o-SWCNT DFT scenarios. Further analysis revealed that this is a consequence of the dominating polar binding contribution that mainly determines the absolute energy distance AED .

Table 3 Two-dimensional solubility parameters and of selected (o-)MWCNT and small probe molecules (* = HSP values predicted) in comparison with computational binding energies.

				E_{ads} [eV]	
	δ_D [MPa ^{1/2}]	δ_a [MPa ^{1/2}]	R [MPa ^{1/2}]	SWCNT	o-SWCNT
MWCNT	20.5	7.5	3.9	-1.44	
o-MWCNT (90 min)	15.4	20.8	7.9	-0.29	
Cyclohexane	16.8	0.2	-	-0.37	-0.13
Cyclohexanol	17.4	14.1	-	-0.35	-0.38
Methoxycyclohexane*	16.5	5.0	-	-0.49	-0.47
Benzene	18.4	2.0	-	-0.45	-0.12
Phenol	18.5	16.0	-	-0.50	-0.16
Anisol	17.8	8.2	-	-0.59	-0.14

**Figure 7** (a) Plot of total adsorption energies absolute energy distance AED against E_{ads} for both pristine (filled circles) and oxidized (unfilled diamonds) systems. The latter has been least-square fitted with a linear equation. (b) Correlation between

δ_a^2 and $\frac{E_{polar}}{V_{benzene}} E_{polar}$ and with being derived from o-SWCNT. The datapoints for methoxycyclohexane - indicated by triangles

- are treated as outliers due to lack of reliable HSP data.

Our combined experimental and theoretical study showed that clear trends can be delineated for the solubility of oxidized carbon nanotubes: While the introduction of OH-functions to MWCNT enables CNT-lignin interaction through hydrogen bonding it diminishes dispersive interactions that dominate at early oxidation stages. With increasing functionalization density, the CNT- π -system becomes inaccessible and the main mode of interaction slowly changes to hydrogen bonding interactions. At all oxidation stages, the CNT reaggregation is severely impeded, thus favoring CNT-lignin interaction.

ACKNOWLEDGMENTS

This research, carried out in line with the project "CARBOPREC – Renewable source nanostructured precursors for carbon fibers," was funded within the 7th Framework Programme of the European Union (grant No. 604215). We gratefully acknowledge the computational resources from FZ Jülich (project HFR08). Finally, we acknowledge the generous supply of organosolv lignin and MWCNT from Fraunhofer CBP (Leuna, Germany) and Arkema (Région de Pau, France) respectively.

REFERENCES

1. E. Frank, L.M. Steudle, D. Ingildeev, J.M. Spörl, and M.R. Buchmeiser, Carbon fibers: Precursor systems, processing, structure, and properties. *Angew. Chem. Int. Ed.* **53**, 5262–5298 (2014).
2. D.A. Baker and T.G. Rials, Recent advances in low-cost carbon fiber manufacture from lignin. *J. Appl. Polym. Sci.* **130**, 713–728 (2013).
3. C.W. Dence and S.Y. Lin, Introduction, in S.Y. Lin and C.W. Dence (Eds.), *Methods in Lignin Chemistry*, chap. 1, pp. 3–19, Springer, Berlin (1992).
4. C. Heitner, D. Dimmel, and J.A. Schmidt (Eds.), *Lignin and Lignans*, p. 651, Taylor & Francis, Boca Raton, FL (2010).
5. K.V. Sarkanen and C.H. Ludwig (Eds.), *Lignins*, p. 916, Wiley-Interscience, New York (1971).
6. I. Delidovich, P.J.C. Hausoul, L. Deng, R. Pfitzenreuter, M. Rose, and R. Palkovits, Alternative monomers based on lignocellulose and their use for polymer production. *Chem. Rev.* **116**, 1540–1599 (2016).
7. O. Faruk and M. Sain (Eds.), *Lignin in Polymer Composites*, p. 249, Elsevier, Boston MA (2016).
8. G. Brunow and K. Lundquist, Functional groups and bonding patterns in lignin (including lignin-carbohydrate complexes), in C. Heitner, D. Dimmel, and J.A. Schmidt (Eds.), *Lignin and Lignans*, pp. 267–299, Taylor & Francis, Boca Raton, FL (2010).
9. F.S. Baker, D.A. Baker, and P.A. Menchofer, Carbon nanotube (cnt)-enhanced precursor for carbon fiber production and method of making a cnt-enhanced continuous lignin fiber, 1469379462984916246-US Patent 20110285049A1, assigned to UT-Battelle LLC (11/24/2011).
10. J.N. Coleman, U. Khan, W.J. Blau, and Y.K. Gun'ko, Small but strong: A review of the mechanical properties of carbon nanotube–polymer composites. *Carbon* **44**, 1624–1652 (2006).
11. M. Monthieux and V.L. Kuznetsov, Who should be given the credit for the discovery of carbon nanotubes? *Carbon* **44**, 1621–1623 (2006).
12. L.V. Radushkevich and V.M. Lukynovich, O strukture ugleroda, obrazujucesja pri termiceskom razlozenii okisi ugleroda na zeleznom kontakte. *Zurn. Fisic. Chim.* **26**, 88–95 (1952).
13. S. Iijima, Helical microtubules of graphitic carbon. *Nature* **354**, 56–58 (1991).
14. Y. Liu and S. Kumar, Polymer/carbon nanotube nano composite fibers—A review. *ACS Appl. Mater. Interfaces* **6**, 6069–6087 (2014).
15. H.C. Liu, A.-T. Chien, B.A. Newcomb, Y. Liu, and S. Kumar, Processing, structure, and properties of lignin- and CNT-incorporated polyacrylonitrile-based carbon fibers. *ACS Sustainable Chem. Eng.* **3**, 1943–1954 (2015).
16. N.-Y. Teng, I. Dallmeyer, and J.F. Kadla, Incorporation of multiwalled carbon nanotubes into electrospun softwood kraft lignin-based fibers. *J. Wood Chem. Technol.* **33**, 299–316 (2013).
17. J. Andzelm, N. Govind, and A. Maiti, Nanotube-based gas sensors – Role of structural defects. *Chem. Phys. Lett.* **421**, 58–62 (2006).
18. D.A. Britz and A.N. Khlobystov, Noncovalent interactions of molecules with single walled carbon nanotubes. *Chem. Soc. Rev.* **35**, 637–659 (2006).
19. V. Gayathri and R. Geetha, Hydrogen adsorption in defected carbon nanotubes. *Adsorption* **13**, 53–59 (2007).
20. G. Lugo, I.G. Cuesta, J. Sanchez Marin, and A. Sanchez de Meras, MP2 study of physisorption of molecular hydrogen onto defective nanotubes: Cooperative effect in Stone-Wales defects. *J. Phys. Chem. A* **120**, 4951–4960 (2016).
21. E. Munusamy and S.E. Wheeler, Endohedral and exohedral complexes of substituted benzenes with carbon nanotubes and graphene. *J. Chem. Phys.* **139**, 94703 (2013).
22. F. Tournus and J.-C. Charlier, Ab initio study of benzene adsorption on carbon nanotubes. *Phys. Rev. B* **71**, 165421 (2005).
23. R.M. Kumar, M. Elango, and V. Subramanian, Carbohydrate-aromatic interactions: The role of curvature on XH- π interactions. *J. Phys. Chem. A* **114**, 4313–4324 (2010).
24. K. Lee, H.J. Lim, S.J. Yang, Y.S. Kim, and C.R. Park, Determination of solubility parameters of single-walled and double-walled carbon nanotubes using a finite-length model. *RSC Adv.* **3**, 4814–4820 (2013).
25. S.W. Kim, T. Kim, Y.S. Kim, H.S. Choi, H.J. Lim, S.J. Yang, and C.R. Park, Surface modifications for the effective dispersion of carbon nanotubes in solvents and polymers. *Carbon* **50**, 3–33 (2012).
26. Z. Spitalsky, D. Tasis, K. Papagelis, and C. Galiotis, Carbon nanotube–polymer composites: Chemistry,

- processing, mechanical and electrical properties. *Prog. Polym. Sci.* **35**, 357–401 (2010).
27. S. Kundu, Y. Wang, W. Xia, and M. Muhler, Thermal stability and reducibility of oxygen-containing functional groups on multiwalled carbon nanotube surfaces: A quantitative high-resolution XPS and TPD/TPR study. *J. Phys. Chem. C* **112**, 16869–16878 (2008).
 28. C. Li, D. Wang, T. Liang, X. Wang, J. Wu, X. Hu, and J. Liang, Oxidation of multiwalled carbon nanotubes by air: benefits for electric double layer capacitors. *Powder Technol.* **142**, 175–179 (2004).
 29. L. Valentini, C. Cantalini, L. Lozzi, I. Armentano, J.M. Kenny, and S. Santucci, Reversible oxidation effects on carbon nanotubes thin films for gas sensing applications. *Mater. Sci. Eng. C* **23**, 523–529 (2003).
 30. L. Valentini, L. Lozzi, C. Cantalini, I. Armentano, J.M. Kenny, L. Ottaviano, and S. Santucci, Effects of oxygen annealing on gas sensing properties of carbon nanotube thin films. *Thin Solid Films* **436**, 95–100 (2003).
 31. S.D.F. Brandão, D. Andrada, A.F. Mesquita, A.P. Santos, H.F. Gorgulho, R. Paniago, M.A. Pimenta, C. Fantini, and C.A. Furtado, The influence of oxygen-containing functional groups on the dispersion of single-walled carbon nanotubes in amide solvents. *J. Phys. Condens. Matter* **22**, 334222 (2010).
 32. S. Detriche, J.B. Nagy, Z. Mekhalif, and J. Delhalle, Surface state of carbon nanotubes and Hansen solubility parameters. *J. Nanosci. Nanotechnol.* **9**, 6015–6025 (2009).
 33. G. Milczarek, Kraft lignin as dispersing agent for carbon nanotubes. *J. Electroanal. Chem.* **638**, 178–181 (2010).
 34. N.-Y. Teng, I. Dallmeyer, and J.F. Kadla, Effect of soft-wood kraft lignin fractionation on the dispersion of multiwalled carbon nanotubes. *Ind. Eng. Chem. Res.* **52**, 6311–6317 (2013).
 35. P.J. Flory, Thermodynamics of high polymer solutions. *J. Chem. Phys.* **9**, 660 (1941).
 36. M.L. Huggins, Solutions of long chain compounds. *J. Chem. Phys.* **9**, 440 (1941).
 37. J. Hildebrand and R.L. Scott, *The Solubility of Nonelectrolytes*, 3rd ed., Reinhold, New York (1950).
 38. C.M. Hansen, *Hansen Solubility Parameters*, 2nd ed., CRC Press, Boca Raton (2007).
 39. E. Stefanis and C. Panayiotou, Prediction of Hansen solubility parameters with a new group-contribution method. *Int. J. Thermophys.* **29**, 568–585 (2008).
 40. J. Enkovaara, C. Rostgaard, J.J. Mortensen, J. Chen, M. Duřak, L. Ferrighi, J. Gavnholt, C. Glinsvad, V. Haikola, H.A. Hansen, H.H. Kristoffersen, M. Kuisma, A.H. Larsen, L. Lehtovaara, M. Ljungberg, O. Lopez-Acevedo, P.G. Moses, J. Ojanen, T. Olsen, V. Petzold, N.A. Romero, J. Stausholm-Møller, M. Strange, G.A. Tritsarlis, M. Vanin, M. Walter, B. Hammer, H. Häkkinen, G.K. Madsen, R.M. Nieminen, J.K. Nørskov, M. Puska, T.T. Rantala, J. Schiøtz, K.S. Thygesen, K.W. Jacobsen, Electronic structure calculations with GPAW: A real-space implementation of the projector augmented-wave method. *J. Phys. Condens. Matter* **22**, 253202 (2010).
 41. J.J. Mortensen, L.B. Hansen, and K.W. Jacobsen, Real-space grid implementation of the projector augmented wave method. *Phys. Rev. B* **71**, 035109 (2005).
 42. J.P. Perdew, K. Burke, and M. Ernzerhof, Generalized gradient approximation made simple. *Phys. Rev. Lett.* **77**, 3865–3868 (1996).
 43. A. Tkatchenko and M. Scheffler, Accurate molecular van der Waals interactions from ground-state electron density and free-atom reference data. *Phys. Rev. Lett.* **102**, 73005 (2009).
 44. M. Monthuoux, Filling single-wall carbon nanotubes. *Carbon* **40**, 1809–1823 (2002).
 45. P. Hobza, J. Hirst, K.D. Jordan, C. Lim, K. Müller-Dethlefs, and W. Thiel, *Non-Covalent Interactions*, Royal Society of Chemistry, Cambridge (2009).
 46. C.A. Hunter and J.K. Sanders, The nature of π - π interactions. *J. Am. Chem. Soc.* **112**, 5525–5534 (1990).
 47. D. Umadevi, S. Panigrahi, and G.N. Sastry, Noncovalent interaction of carbon nanostructures. *Acc. Chem. Res.* **47**, 2574–2581 (2014).
 48. M. Hassan, M. Walter, and M. Moseler, Interactions of polymers with reduced graphene oxide: van der Waals binding energies of benzene on graphene with defects. *Phys. Chem. Chem. Phys.* **16**, 33–37 (2014).
 49. R. Eisenschitz and F. London, Über das Verhältnis der van der Waalsschen Kräfte zu den homöopolaren Bindungskräften. *Z. Phys.* **60**, 491–527 (1929).
 50. D.W. van Krevelen and K. te Nijenhuis, *Properties of Polymers*, 4th ed., p. 1004, Elsevier, Amsterdam (2009).
 51. A. Held and M. Walter, Simplified continuum solvent model with a smooth cavity based on volumetric data. *J. Chem. Phys.* **141**, 174108 (2014).

Supplementary Document Available Online

http://www.scribenerpublishing.com/images/JRM/JRM-2017-0067/jrm_JRM-2017-0067_supp1.docx